Precision Engineering 48 (2017) 164–171

Contents lists available at ScienceDirect

Precision Engineering

journal homepage: www.elsevier.com/locate/precision

In-process estimation of fracture surface morphology during wheel scribing of a glass sheet by high-speed photoelastic observation

Ryohei Hasegawa [a], Souta Matsusaka [a,*], Hirofumi Hidai [a], Akira Chiba [a], Noboru Morita [a], Takashi Onuma [b]

[a] Department of Mechanical Engineering, Chiba University, 1-33, Yayoi-cho, Inage-ku, Chiba, 263-8522, Japan
[b] Photron Ltd., 1-105, Kanda Jinbo-cho, Chiyoda-ku, Tokyo, 101-0051, Japan

ARTICLE INFO

Article history:
Received 18 November 2016
Accepted 28 November 2016
Available online 15 December 2016

Keywords:
Non-alkali glass
Mechanical cleavage
Scribing wheel
High-speed imaging
Birefringence phase difference measurement
Fracture surface morphology

ABSTRACT

Defect-free glass separation techniques are in strong demand in glass processing industries. In this study, we intended to observe the internal stress field during/after wheel scribing of a glass sheet using the photoelastic method. First, we visualized the crack propagation behavior in a 0.7-mm-thick non-alkali glass sheet during mechanical scribing with a 2.0-mm-diameter serrated diamond wheel using high-speed imaging techniques. The observation results under various applied load conditions showed that the crack propagation behavior changed dramatically at a load of approximately 9–10 N; the generated crack hardly propagated in the thickness direction under lower load conditions, in contrast to the rapid propagation under higher load conditions. The fracture surface morphology that was observed after cleavage also changed, from damaged to defect-free surfaces with increments in the applied load around the transition point (9–10 N). This result indicated that the fracture surface morphology was determined by the crack propagation behavior. Second, the birefringence phase difference was measured from the upper side of the glass sheet to enable understanding of the stress fields induced by scribing wheel indentations. As a result, the phase differences that were distributed along the scribe line were shown to differ depending on the applied loads; the phase difference changed little under lower load conditions, but vanished immediately under higher load conditions. Therefore, these differences were dependent on whether or not rapid crack propagation occurred. The measured phase difference distribution thus included information about the crack propagation behavior, and this information could be used as a criterion for estimation of the fracture surface morphology. An in-process estimation method for the fracture surface morphology during mechanical wheel scribing was therefore developed based on high-speed polarization imaging techniques.

1. Introduction

Thin silicate glass sheets are widely used in electric devices, including use as glass substrates for liquid crystal displays [1] and as glass interposers in three-dimensional integrated circuits [2]. For industrial use, it is necessary for a large mother glass substrate to be divided into smaller parts with the intended sizes and configurations. Recently, demand for high quality separation techniques for glass sheets have been increasing, because even invisibly small defects such as micro-cracks on separated glass edges can severely degrade the bending strength of glass sheets [3]. At present, mechanical cleavage techniques based on the use of diamond scribing wheels are commonly used to separate glass sheets [4,5]. In these methods, the separation procedure generally consists of two steps: crack generation and propagation in a glass sheet by mechanical force (scribing), and then separation by a bending force (breaking). Because crack propagation is accompanied by stress concentration and relaxation [6], the fracture surface morphology is strongly dependent on the stress field induced in the glass sheet by the applied load delivered by the scribing wheel. Therefore, correct understanding of the internal stress field during the scribing process is critically important for defect-free cleavage. There are two potential approaches to analysis of this field: (i)

* Corresponding author.
E-mail addresses: aaya2390@chiba-u.jp (R. Hasegawa), matusaka@faculty.chiba-u.jp (S. Matsusaka), hidai@faculty.chiba-u.jp (H. Hidai), achiba@chiba-u.jp (A. Chiba), nmorita@chiba-u.jp (N. Morita), oonuma@photron.co.jp (T. Onuma).

http://dx.doi.org/10.1016/j.precisioneng.2016.11.017
0141-6359/

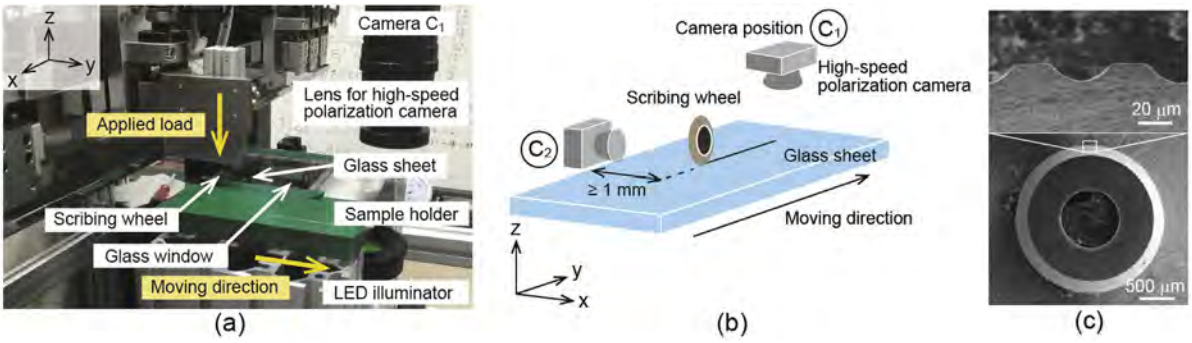

Fig. 1. Experimental setup used for wheel scribing of glass sheet. (a) Appearance of wheel scriber; (b) camera position for high-speed observation; (c) SEM image of scribing wheel notched on the ridge line.

numerical analysis using the finite element method (FEM), which was applied successfully to the laser scribing process [7,8], and (ii) photoelastic observation, which can visualize an elastic stress-induced birefringence distribution in transparent materials [9]. In this study, the photoelastic approach has been adopted.

Photoelastic observation is conventionally used to understand the stress distributions in transparent materials under an anisotropic stress field. The birefringence phase difference is proportional to the difference between the two principal stresses with a photoelastic constant [9]. The birefringence phase difference distributions around internal cracks have been investigated previously, e.g., as shown by Colombo and Guagliano [10]. However, the currently established observation methods are difficult to apply to dynamic phenomena because their polarization devices use mechanical or electrical modulators. Recently, one of the authors developed a high-speed photoelastic observation method by combining a pixelated polarizer array with a high-speed image sensor [11]. This system is similar to the methods proposed by Sakaue et al. [12] and Yoneyama and Sakaue [13], but more frequent imaging (theoretical maximum frequency of 1.3 MHz) is possible when using a parallel read-out electric circuit for the high-speed image sensor. In our previous paper [14], we observed the change in the phase difference distribution in a glass sheet during wheel scribing from the direction of travel (i.e., far from the front of the crack being generated). This result indicated that the stress field fluctuation was closely related to the crack propagation behavior. However, it was difficult to measure the phase difference immediately adjacent to the generated crack, because the measured phase difference was an integrated value along the entire scribe line. To clarify the stress field fluctuation with crack propagation, an in-situ measurement of the internal phase difference from the upper side of the glass sheet is a reasonable approach.

In this study, we investigated the effect of the applied load on both the crack propagation behavior and the fracture surface morphology. Simultaneously, the phase difference distribution around the propagating crack was measured from the upper side of the glass sheet. We then discussed the fracture surface morphology relative to the characteristic stress field fluctuation with/without crack propagation. These findings enable in-process estimation of the fracture surface morphology during wheel scribing.

2. Experiments

Fig. 1(a) and (b) show the appearance and a schematic illustration of the wheel scriber (MM5050A2, Mitsuboshi Diamond Industrial (MDI), Osaka, Japan) that was used in the experiments. In this setup, the scribing wheel moved only in z-direction and the glass sample was moved on a linear stage in y-direction. Two high-speed polarization cameras (MC2.1, Photron, Tokyo, Japan; frame rate: ~2 kHz) were placed at positions C_1 and C_2, as shown in Fig. 1(b). Camera C_2 was used in a normal mode, i.e., the birefringence phase difference was not measured. In this experiment, the viewing fields of C_1 and C_2 cameras were $0.5 \times 0.5\,mm^2$ and $2.1 \times 2.1\,mm^2$, respectively. The focal points of two cameras were at the glass surface for C_1 and at the glass inside just beneath the scribing wheel for C_2. The scribing experiment was performed using a diamond wheel with notches on the ridge line (Penett-SDX, MDI; diameter: 2.0 mm; edge angle: 125°; 110 notches). A scanning electron microscope (SEM) image of this wheel is shown in Fig. 1(c). During observation of the crack propagation behavior from position C_2, it was preferred that the scribe line was located near the glass edge. However, when the margin from the edge was insufficient, the scribing phenomena were likely to differ from the case in which the wheel traveled along the central area. Therefore, the margin between the glass edge and the scribe line was set to be larger than 1 mm (see Fig. 1(b)). A 0.7-mm-thick alkali-free boroaluminosilicate glass sheet (Code 1737, Corning, Corning, NY; $10 \times 30\,mm^2$) was used in the experiments. In our previous paper [14], we reported that the scribing speed had little influence on both the crack propagation behavior and the fracture surface morphology. The scribing speed was therefore fixed at 30 mm/s. The scribing wheel contacted to a glass sheet with applied load at stage position S_1 in Fig. 2, and 15 mm of crack was formed by the moving of linear stage from S_1 to S_2. The applied load was varied from 5 to 20 N. The scribing wheel was detached from the glass surface when the linear stage reached at S_2.

In the photoelastic observation from the upper side of the glass sheet, it was necessary to apply illumination from the opposite side. For this purpose, a glass window (3-mm-thick borosilicate glass) was prepared in the sample holder, as shown in Fig. 2. The light-emitting diode (LED) illuminator wavelength was 520 nm. Unfortunately, the glass sheet immediately underneath the scribing wheel could not be observed, because the wheel and the wheel driver acted to screen the glass sample. Therefore, the photoelastic observation was performed when the linear stage moved to the position S_4 by passing between the high-speed polarization camera and the illuminator (i.e., at the stage position S_3 between S_2 and S_4, as shown in Fig. 2). The distance between the scribing wheel and the high-speed camera was 150 mm, and the photoelastic images obtained showed a phase difference distribution of approximately 5 s after the scribing wheel passed over the glass surface. As described above, in this experiment, the wheel load was not applied at the time when the photoelastic observation was performed at S_3. However, we believe that the absence of the applied load had little influence on the phase difference at the observation point, because the distance between the wheel and the camera was sufficiently large. The phase difference obtained was thus considered to be that which occurred during wheel scribing with the applied load.

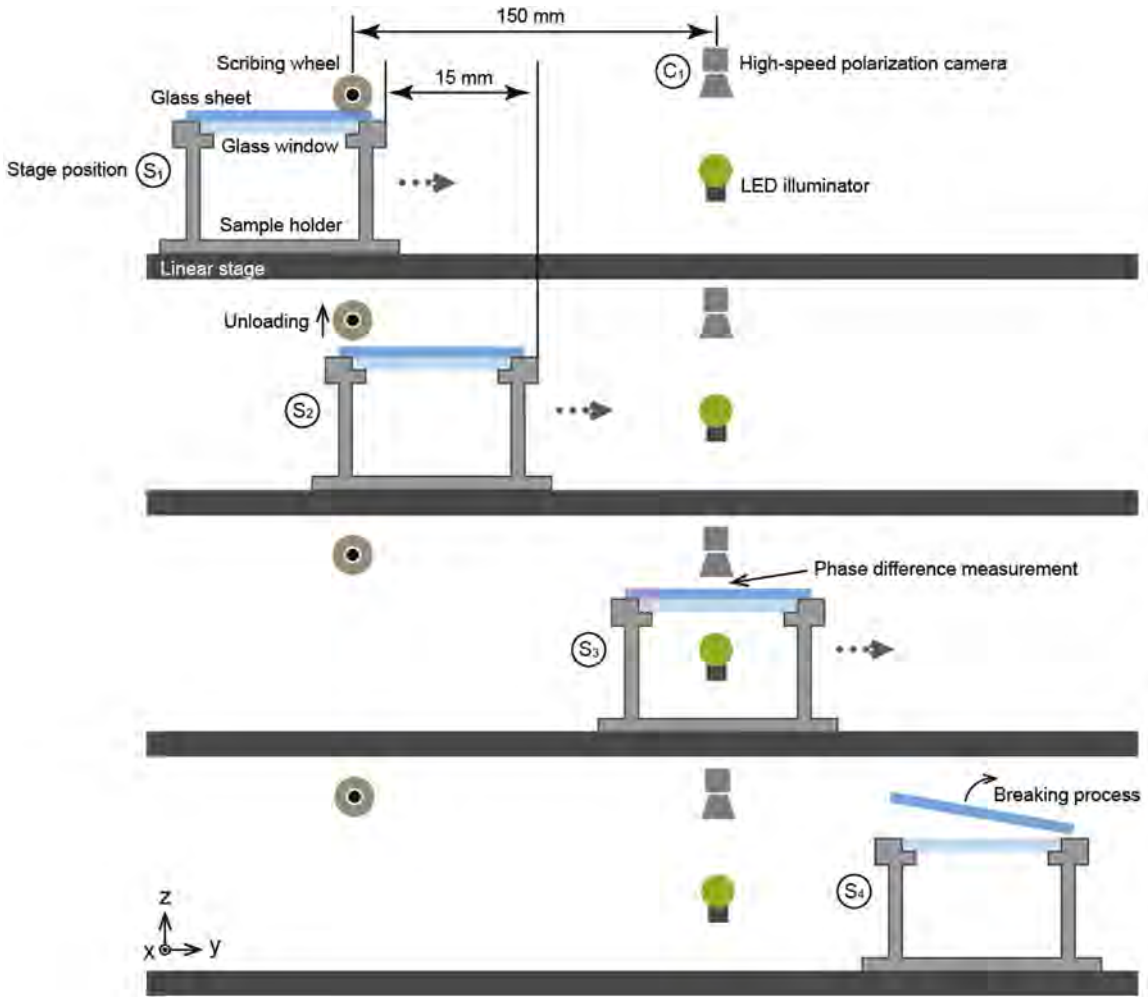

Fig. 2. High-speed method for measurement of phase difference from upper side of glass sheet. For illumination, a glass window is prepared in the sample holder. It should be noted that the stage positions S_1, S_2, S_3 and S_4 are on the same line.

After the linear stage reached to the position S_4, the glass sheets were hand-broken within 5 min of completion of scribing for observation of the fracture surface by optical microscopy.

3. Results and discussion

3.1. Crack propagation and fracture surface morphology

Fig. 3(a) shows an image captured around the contact area between the scribing wheel and the glass sheet that was obtained from high-speed camera C_2. The blurred stripe pattern under the wheel indicates a propagating crack [15]. In Fig. 3(b) and (d), the traced crack shapes are illustrated for applied loads of 9 and 18 N. As shown in these figures, the applied load of 18 N produced a deep crack with a characteristic shoulder; this was in contrast to the 9 N case, in which very slow crack propagation was observed. In this paper, the first stage of the propagating crack at 18 N is called a 'median crack' according to the references [1,16]. Fig. 3(c) and (e) show optical micrographs of the cleaved surfaces that were scribed at 9 and 18 N, respectively. In the lower load case, a hackle-mark with irregular cracks appeared near the scribed surface. In contrast, a rib-mark with periodic Wallner lines was observed under the higher load condition. Comparison between Fig. 3(d) and (e) showed that the median crack depth corresponded directly to the rib-mark depth. It was also shown that scribing without the median crack propagation produced a damaged fracture surface.

To understand the threshold load for median crack propagation, the relationship between the applied load and the median crack depth was investigated. The results of this study are shown in Fig. 4. In the figure, the fracture surface morphology under every applied load is indicated using solid symbols. Fig. 4 shows that the dramatic transition in the median crack depth occurs at an applied load of approximately 9–10 N, and it accompanies a change in the fracture pattern. While we do not fully understand the reasons for these dramatic changes, a promising candidate explanation is proposed as follows. The scribing wheel that was used in this experiment has serrations on the ridge line, as shown in Fig. 1(c). Therefore, some contact points (3–5 points under our experimental conditions) were formed between the scribing wheel and the glass sheet by application of the load. The compressive stress field surrounded by a tensile field was of course formed immediately under each tooth of the scribing wheel, resulting in the generation of a small crack. In the higher load case, these small cracks instantly combined to form a median crack by superposition of the neighboring tensile stress fields. Therefore, the rib-mark that was imprinted on the fracture surface was considered to be the result of the continuous generation of median cracks. In contrast, under the lower load conditions, the tensile stresses that formed were so small that the stress intensity factor around the crack tip was lower than the fracture toughness. Therefore, the connection between the small cracks did not occur under these conditions. In this case, many irregular cracks were generated around the initial small cracks to release the

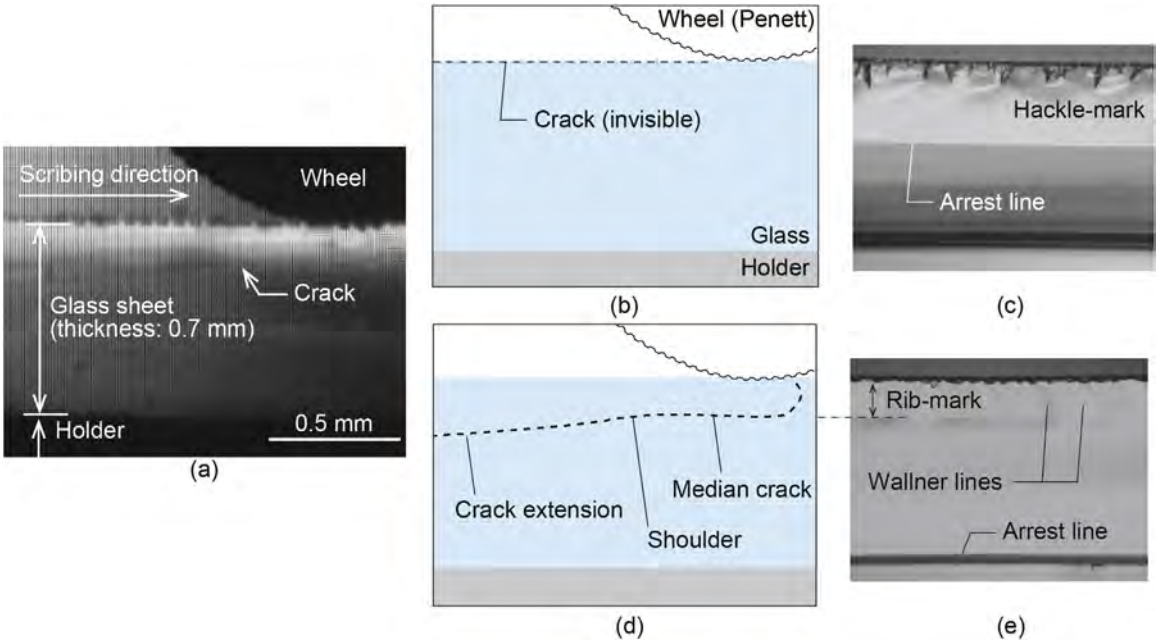

Fig. 3. Crack propagation behavior immediately below the rotating scribing wheel. (a) Captured image from high-speed camera; (b) and (d) traced crack shapes under applied loads of 9 and 18 N, respectively; (c) and (e) optical micrographs of cleaved surfaces scribed under loads of 9 and 18 N, respectively.

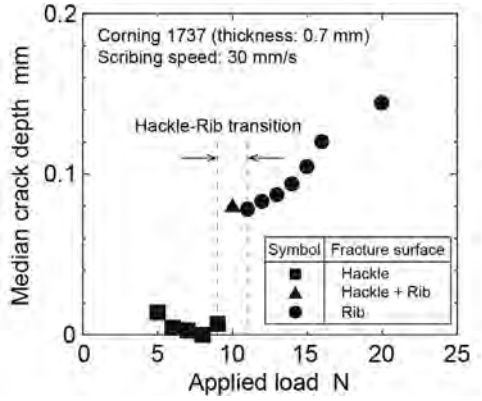

Fig. 4. Effects of applied load on median crack depth. The fracture surface morphology (hackle and/or rib-mark) under each applied load is also indicated using solid symbols.

strain energy by creating an increased surface area; as a result, the cleaved surface exhibited a damaged appearance.

3.2. Photoelastic observation

As described above, the median crack propagation and the fracture surface morphology are closely related to the internal stress field around the initial cracks. To understand the stress distribution just after scribing, photoelastic observation was performed from the upper side of the glass sheet. Fig. 5 shows the captured images of the surface appearance and the measured phase difference that was obtained using high-speed polarization camera C_1 when the applied loads were 9 and 18 N. The frame rate was 250 Hz. Fig. 5(a) and (c) show that there are few differences between the two appearances; however, the phase difference distributions shown in Fig. 5(b) and (d) were different. When the applied load was 9 N, a phase difference of over 6 nm (from light blue to red pixels in Fig. 5(b)) was distributed in a 0.06 mm zone along the scribe line. In the 18 N case, the phase difference distribution was considerably narrowed (~0.03 mm).

To provide a detailed observation, phase difference measurements were performed using a glass sheet fixed between the camera and the illuminator (i.e., the linear stage was stopped at S_3 position shown in Fig. 2). The phase difference distributions observed 5 s after scribing are shown in Fig. 6(a) and (c). In addition, the corresponding distributions measured 3.6 ks (1 h) after scribing are also shown in Fig. 6(b) and (d). Essentially, Fig. 6(a) and (c) should coincide with Fig. 5(b) and (d), respectively. The reason for the observed disagreement between the figures was that the frame rate of 250 Hz, which was limited by the size of the visual field and the illumination light intensity, was insufficient for phase difference measurements in the moving glass sheet. This problem will be solved in future work by preparing a light source with sufficient intensity to perform the high-speed measurements. As shown in Fig. 6(a), the periodic phase difference, which had a pitch that corresponded exactly to the tooth pitch of the scribing wheel, appeared in the case of the 9 N applied load. A pair of semicircular distributions formed around the tooth indentation point. This result indicated that the residual stress distribution still existed, even 5 s after scribing, when the applied load was low. This phase difference distribution gradually disappeared in the period up to 3.6 ks afterwards (Fig. 6(b)). In contrast, the characteristic phase difference distribution was not observed in Fig. 6(c), and there was little change in the appearance of the distribution (Fig. 6(d)). This result indicated that the stress distribution caused by the wheel indentation had vanished 5 s after the scribing process. With reference to Fig. 3 (d), we believe that the rapid median crack propagation observed under high applied load conditions simultaneously involves rapid relaxation of the residual stress field.

At present, we cannot determine the three dimensional stress distribution generated in a scribed glass sheet only by the obtained phase differences. The reasons are as follows; the phase difference is merely proportional to the difference between two principal stresses in x-y plane perpendicular to the illumination light axis (z-direction), and the measured phase difference is integrated value of phase difference at every thin plane along z axis. However, here we found that the rotating wheel induced a highly anisotropic stress field around the formed crack, which may be due to the large tensile stress in x-direction resulting in crack opening and small

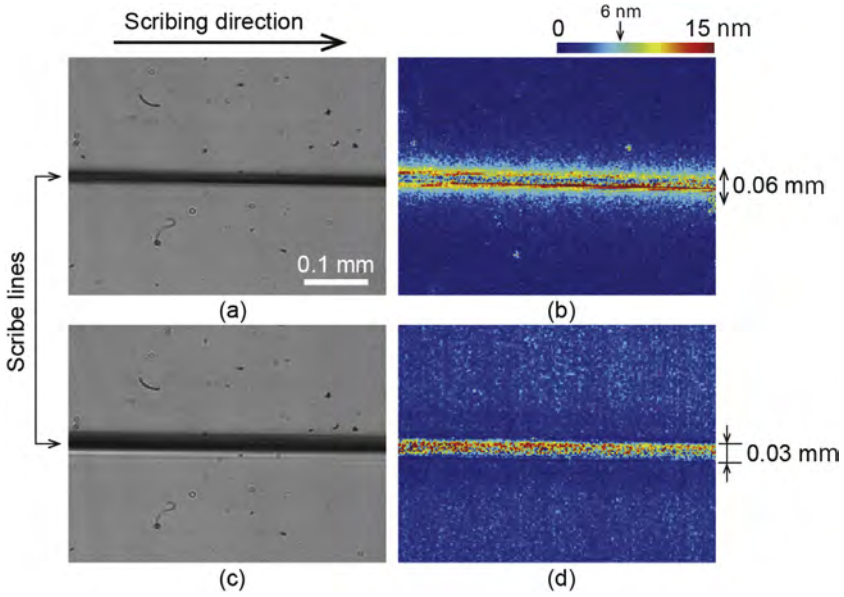

Fig. 5. High-speed observation images from the upper side of the moving glass sheet. The frame rate was 250 Hz. (a) and (c) Captured images of surfaces scribed under loads of 9 and 18 N, respectively; (b) and (d) measured phase difference distributions under loads of 9 and 18 N, respectively. Color scale range of the phase difference in (b) and (d) is 0–15 nm.

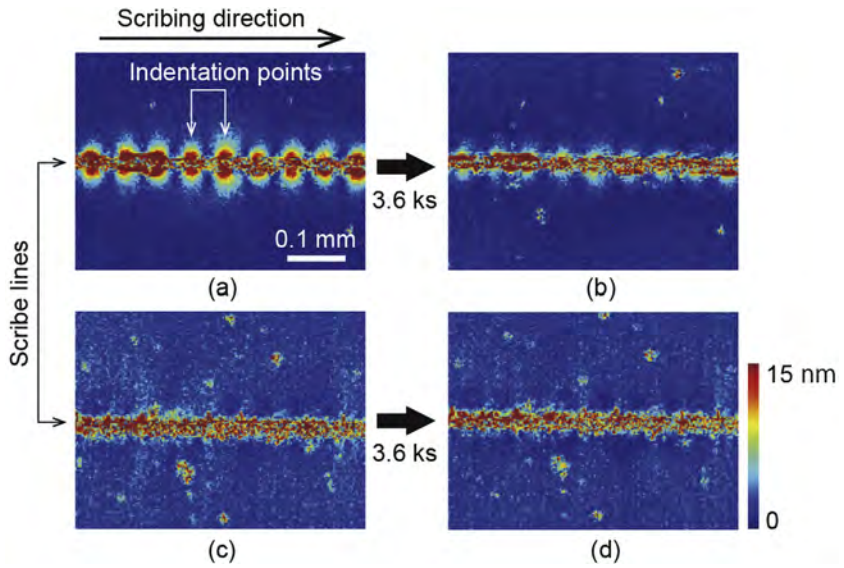

Fig. 6. Phase difference distribution from the upper side of the spatially fixed glass sheet. (a) and (c) Distributions at 5 s after scribing under loads of 9 and 18 N, respectively; (b) and (d) distributions at 3.6 ks after scribing under loads of 9 and 18 N, respectively.

tensile/compressive stress in y-direction. The cooperative work with the numerical analysis such as FEM will be effective for the deep understanding of three dimensional stress filed.

3.3. In-process estimation of the fracture surface morphology by high-speed phase difference measurements

Based on the discussion in the previous sections, it was proposed that the residual phase difference that was distributed around the scribe line was determined by the median crack propagation behavior, which was in turn closely related to the fracture surface morphology. Therefore, the characteristics of the phase difference distributions can be used as estimation criteria for the fracture surface morphology. For analysis purposes, the phase difference distribution maps were drawn according to the following procedure (shown in Fig. 7). A measurement line was defined at the center of the viewing field (between the white arrows) on each captured image that was obtained from the high-speed polarization camera. The phase difference distributions on the measurement line were stacked in chronological order and were then combined into one image. This image then shows the phase difference distribution immediately below the polarization camera (i.e., at 5 s after scribing).

Fig. 8(a)–(c) show the phase difference maps measured when the applied loads were 9, 10, and 18 N, respectively. In these figures, the appearances of the cleaved surfaces are also shown. Under the lowest load condition (Fig. 8(a)), a widely distributed phase difference was measured, and a hackle-mark with irregular cracks was observed on the cleaved surface along the entire scribing length. In contrast, a narrow phase difference distribution and periodic rib-marks were observed under the highest load condition (Fig. 8(c)). Therefore, the width of the phase difference distribution will be

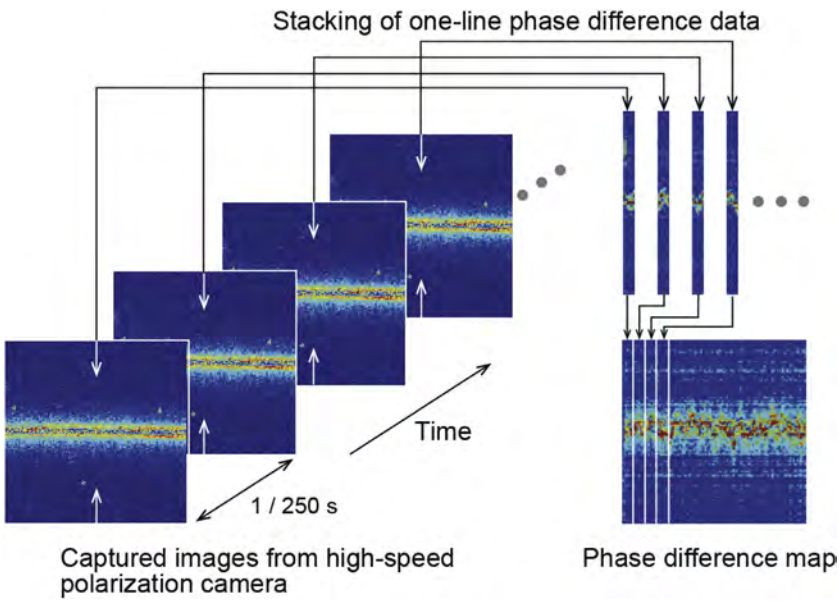

Fig. 7. Drawing procedure for phase difference map. The measured phase difference on the center line of each captured image is stacked in chronological order and combined into one image.

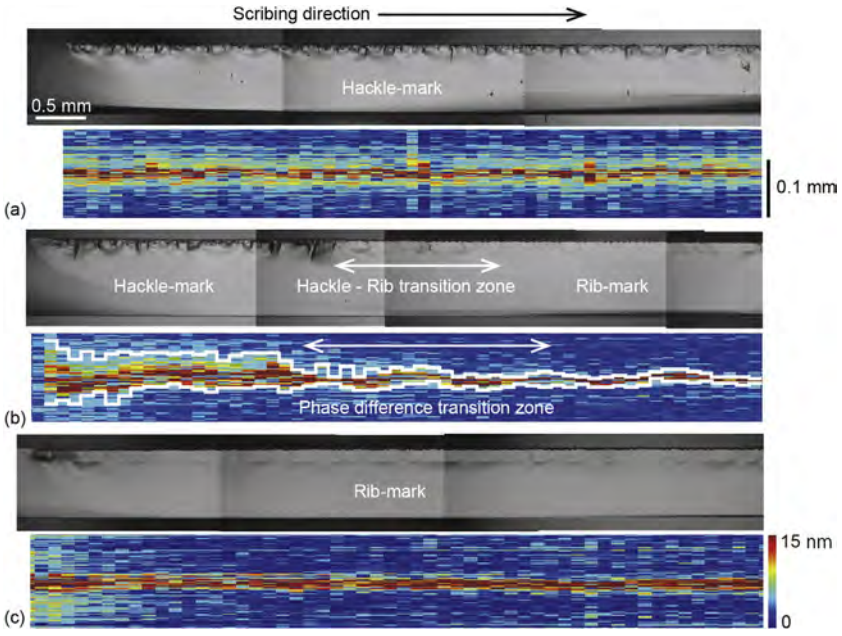

Fig. 8. Comparison between cleaved surface morphologies and phase difference maps. Applied loads of (a) 9 N, (b) 10 N, and (c) 18 N. The area framed by the white line in (b) means that the phase difference is more than 7.5 nm. A transition in surface morphology (from hackle to rib-mark) is observed in (b), along with a transition in the phase difference distribution.

the estimation criterion used for the cleaved surface morphology. Fig. 9 shows the typical phase differences measured on a line perpendicular to the scribe lines at 9 and 18 N. In this case, we can for example determine whether the surface morphology is damaged or defect-free, depending on the criterion where the range of the phase difference over 7.5 nm is greater than 0.03 mm. To provide contrast, the surface morphology transition within a scribe line was observed at 10 N, as shown in Fig. 8(b). Our estimation method proves to be useful even in this case. The high phase difference zone around the scribe line became narrower with the transition in the surface morphology (the area framed by the white line in Fig. 8(b) indicates the area where the phase difference was more than 7.5 nm). When the criterion that the range of the phase difference over 7.5 nm must be within the range from 0.025 to 0.035 mm was adopted, the phase difference transition zone was determined as indicated by the white arrow in Fig. 8(b). Comparison between the surface morphology and the phase difference distribution showed that the surface morphology transition zone agreed well with the phase difference transition zone.

As described above, the phase difference distribution contains abundant information on the stress field that formed in the glass sheet; therefore, the proposed method will be applicable to the detection of other defects, such as oblique crack propagation or tapered edge formation. For example, Fig. 10 shows that oblique

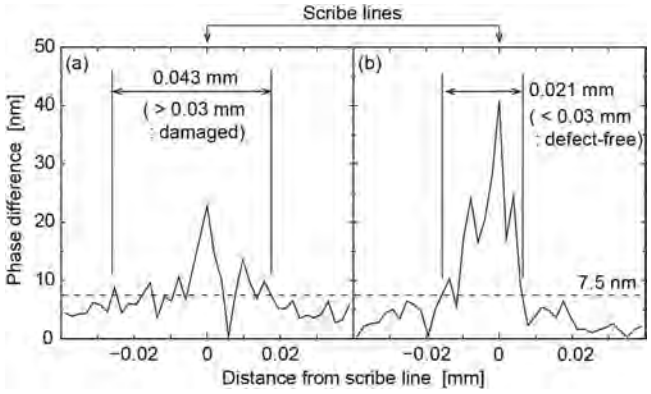

Fig. 9. Typical phase difference distribution on a line perpendicular to the scribe line. Applied loads of (a) 9 N and (b) 18 N. The range of the distributed phase difference over 7.5 nm at 9 N is approximately double that at 18 N.

crack propagation occurred at the end of the scribing process when the scribing wheel traveled close to the edge of the glass sheet. Up to a time of 3.6 ks after scribing, the crack tip moved to the right side of the scribe line. As shown in Fig. 10(c) and (d), we can observe unbalanced phase differences between both sides of the scribe line. It was also observed that the high phase difference on the right side of the scribe line gradually disappeared as the crack propagated. This means that the oblique crack propagation occurred to release the unbalanced residual strain energy. At present, the relationship between the unbalanced phase difference distribution and the oblique crack propagation process is not fully understood. However, estimation of the propagation direction will be enabled by the photoelastic method on the basis of theoretical fracture mechanics [13].

In our experiments, the frame rate of the high-speed polarization camera was 250 Hz. Because a scribing speed of 200–300 mm/s is commonly used in glass processing industries, problems with processed quality can be detected within a few millimeters of scribing. Therefore, the estimation method presented here will be advantageous for improvements in production efficiency.

4. Summary

In this report, the relationship between the crack propagation behavior and the fracture surface morphology during the mechanical wheel scribing of 0.7-mm-thick non-alkali glass sheets was investigated using high-speed imaging techniques. The crack propagation behavior changed dramatically under an applied load of approximately 9–10 N, resulting in transitions in the fracture surface patterns. Birefringence phase difference measurements showed that the crack propagation occurred with/without stress relaxation around the scribe line. The finding that the residual phase difference distribution was determined by the crack propagation behavior indicated that the phase difference information could be used as an estimation criterion for the fracture surface morphology. The proposed system, which consisted of a high-speed polarization camera and associated image processing techniques, enabled in-process estimation of the fracture surface morphology during mechanical wheel scribing. In future work, we intend to investigate the applicability of the proposed method to the detection of other defects and to use with other transparent materials, such as glass substrates with different thicknesses and chemical compositions, chemically-strengthened glasses, and also intend to improve our understanding of the internal stress field during/after scribing.

Acknowledgements

The authors gratefully acknowledge the experimental support of Mitsuboshi Diamond Industrial Co., Ltd and the many fruitful discussions with the company's staff. This work was supported by JSPS KAKENHI [grant number 15H03898].

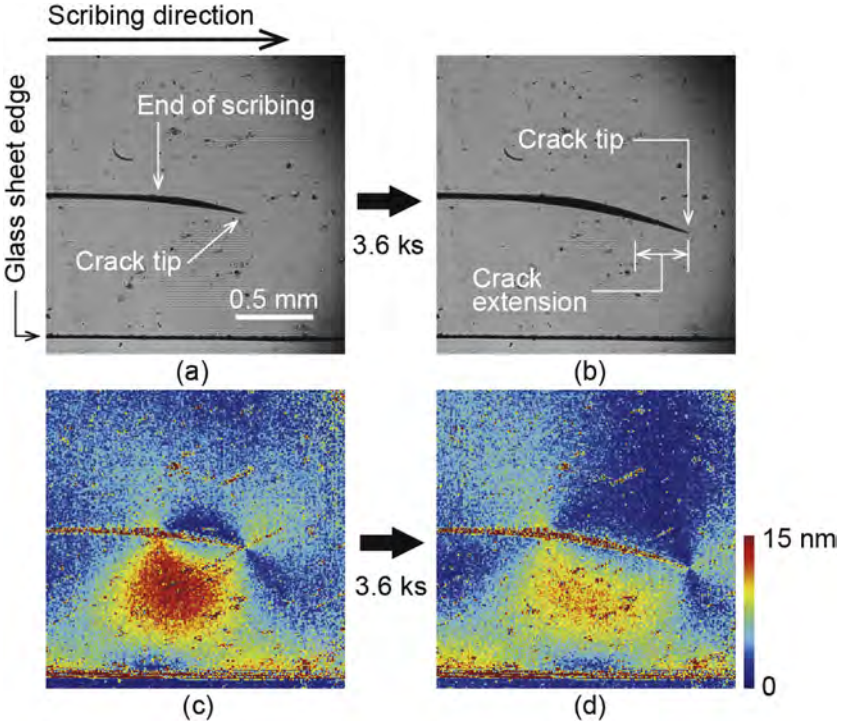

Fig. 10. Oblique crack propagation occurring at the end of scribing. This problem frequently occurs when the scribing wheel travels near the glass sheet edge. (a) and (c) Surface appearance and phase difference distribution 5 s after scribing, respectively; (b) and (d) the corresponding quantities 3.6 ks after scribing.

References

[1] Ono T, Tanaka K. Effect of scribe-wheel dimensions on the cutting of AMLCD glass substrate. J Soc Inf Disp 2001;9:87–94.
[2] Sukumaran V, Bandyopadhyay T. Low-cost thin glass interposers as a superior alternative to silicon and organic interposers for packaging of 3-D ICs. IEEE Trans Compon Packag Manuf Technol 2012;2:1426–33.
[3] Griffith AA. The phenomena of rupture and flow in solids. Phil Trans A 1921;221:163–98.
[4] Tsai CH, Huang BW. Diamond scribing and laser breaking for LCD glass substrates. J Mater Process Technol 2008;198:350–8.
[5] Liao YS, Yang GM, Hsu YS. Effect of geometrical characteristics of a scribing wheel on the bending strength of LCD glass substrates. J Soc Inf Disp 2009;17:287–91.
[6] Okamura H. Introduction to linear elastic fracture mechanics. 1st ed. Tokyo: Baifukan; 1991. p. 57 (in Japanese).
[7] Yamamoto K, Hasaka N, Morita H, Ohmura E. Three-dimensional thermal stress analysis on laser scribing of glass. Prec Eng 2008;32:301–8.
[8] Yamamoto K, Hasaka N, Morita H, Ohmura E. Influence of glass substrate thickness in laser scribing of glass. Prec Eng 2010;34:55–61.
[9] Timoshenko S, Goodier JN. Theory of Elasticity. 2nd ed. New York: McGraw-Hill; 1951. p. 133.
[10] Colombo C, Guagliano M. Photoelastic analysis of cylindrical elements with internal cracks under Hertz contact loading. Fatigue Fract Eng Mater Struct 2010;33:885–96.
[11] Onuma T, Otani Y. A development of two-dimensional birefringence distribution measurement system with a sampling rate of 1.3 MHz. Opt Comm 2014;315:69–73.
[12] Sakaue K, Yoneyama S, Takashi M. Study on crack propagation behavior in a quenched glass plate. Eng Fract Mech 2009;76:2011–24.
[13] Yoneyama S, Sakaue K. Experimental-numerical hybrid stress analysis for a curving crack in a thin glass plate under thermal load. Eng Fract Mech 2014;131:514–24.
[14] Matsusaka S, Mizobuchi G, Hidai H, Chiba A, Morita N, Onuma T. Observation of crack propagation behavior and visualization of internal stress field during wheel scribing of glass sheet. J Jpn Soc Prec Eng 2015;81:270–5 (in Japanese).
[15] Tomei N, Maekawa K, Wakayama H, Tomimori H. A study on scribing with a breakless wheel – observations of crack propagation using a high-speed camera &minus. J Jpn Soc Abrasive Tech 2009;53:684–9 (in Japanese).
[16] Ono T, Pai G, Teng O, Gildea M, Zenteno L, Helfinstine J, et al. Superior cuttability performance of Jade Glass for thin and strong mobile displays. SID Digest 2009;40:1052–5.